Distributed Consensus-Based Model Predictive Control of Inverter Air Conditioners for Voltage Regulation in Distribution Systems

Lunshu Chen, *Student Member, IEEE,* Hongxun Hui, *Senior Member, IEEE,* Yonghua Song, *Fellow, IEEE,* Ye Chen, Wei Feng, *Member, IEEE*

***Abstract*—Distribution system voltage violation problems are receiving more attention due to the high penetration of fluctuating distributed renewable energies. With the development of Internet of Things technologies, demand response is becoming promising to stabilize the distribution system voltage with local demand-side resources. Inverter air conditioners (IACs) account for a large share in demand-side power consumption, which has been widely considered as appropriate resources to provide voltage regulation services for the distribution system by temporally adjusting the power consumption. However, it remains a challenge to schedule large-scale distributed IACs to participate in voltage regulation services considering their complex operation characteristics with both active and reactive powers. To address this problem, this paper proposes a distributed consensus-based model predictive control (DCMPC) algorithm to coordinate the active and reactive power of IACs to participate in voltage regulation. Distributed consensus-based processing allows the IACs to be appropriately scheduled to respond to the regulation signals. The proposed DCMPC algorithm is validated by the realistic IACs aggregated regulation system and hardware-in-the-loop experiments. The experimental results show that the DCMPC algorithm can effectively schedule IACs to keep the voltage operating within the security range and achieve good thermal comfort for customers during voltage regulation.**

***Index Terms*—demand response, distributed model predictive control, hardware-in-the-loop, inverter air conditioners, voltage regulation**

NOMENCLATURE

Abbreviation

DCMPC	Distributed consensus-based model predictive control
DMPC	Distributed model predictive control
DSO	Distribution system operator
ETP	Equivalent thermal parameter
HIL	Hardware-in-the-loop
IoT	Internet of things
MPC	Model predictive control
PCC	Point of common coupling
PV	Photovoltaic
RESs	Renewable energy sources
RTDS	Real-Time digital simulator

Parameter

$\mathbf{S}_{\text{PU}}$	The voltage sensitivity of active power
$\mathbf{S}_{\text{P}\theta}$	The phase angle sensitivity of active power
$\mathbf{S}_{\text{QU}}$	The voltage sensitivity of reactive power
$\mathbf{S}_{\text{Q}\theta}$	The phase angle sensitivity of reactive power
$\Delta\mathbf{P}_{\text{dist}}$	The active power variation at each node
$\Delta\mathbf{Q}_{\text{dist}}$	The reactive power variation at each node
κ_1^{ij}	The coefficients of the IAC's operating power
κ_2^{ij}	The coefficients of the IAC's cooling capacity
ϕ^{ij}	The phase deviation between the voltage and current of the IAC
$\mathbf{J}$	The jacobian matrix
b_1^{ij}	The coefficients of the IAC's operating power
b_2^{ij}	The coefficients of the IAC's cooling capacity
M	The total building number in the distribution system
N	The total room number in a building
$P_{\text{IAC,max}}^{ij}$	The rated active power of the IAC
$Q_{\text{IAC,max}}^{ij}$	The rated reactive power of the IAC
$T_{\max}^{ij}$	The maximum allowable temperature
$T_{\min}^{ij}$	The minimum allowable temperature
$\mathbf{S}_{\text{PU}}^{i}$	The i row of $\mathbf{S}_{\text{PU}}$
$\mathbf{S}_{\text{QU}}^{i}$	The i row of $\mathbf{S}_{\text{QU}}$
$\cos\phi^{ij}$	The power factor of the IAC
$\gamma_{i,\widetilde{i}}$	The communication relationship between building i and building $\widetilde{i}$
$a_{ij,\widetilde{ij}}$	The communication relationship between IAC ij and IAC $\widetilde{ij}$
C_{room}^{ij}	The room's equivalent air heat capacity
R_{room}^{ij}	The equivalent thermal resistance of the room's envelope
$S_{\text{PU}}^{i,\widetilde{i}}$	The voltage sensitivity of active power injection from building i to its neighboring building $\widetilde{i}$
$S_{\text{PU}}^{i,i}$	The voltage sensitivity of building i active power injection
$S_{\text{QU}}^{i,\widetilde{i}}$	The voltage sensitivity of reactive power injection from building i to its neighboring building $\widetilde{i}$
$S_{\text{QU}}^{i,i}$	The voltage sensitivity of building i reactive power

This work is funded in part by the National Natural Science Foundation of China (Grant No. 52407075), in part by the Science and Technology Development Fund, Macau SAR (File no. 0050/2025/AIJ, and File no. 001/2024/SKL), and in part by the Multi-Year Research Grant-General Research Grant 2025 of University of Macau (File no. MYRG-GRG2025-00305-IOTSC). (Corresponding authors: *Hongxun Hui* and *Yonghua Song*).

L. Chen, H. Hui and Y. Song are with the State Key Laboratory of Internet of Things for Smart City and the Department of Electrical and Computer Engineering, University of Macau, Macao, 999078, China, and Hengqin University of Macau Advanced Research Institute, Zhuhai, 519031, China (e-mail: chen.lunshu@connect.um.edu.mo; hongxunhui@um.edu.mo; yhsong@um.edu.mo).

Y. Chen is with the State Grid Jiangsu Electric Power Company Electric Power Research Institute, Nanjing, 211103, China (e-mail: joey_chenye@foxmail.com).

W. Feng is with the Shenzhen Institutes of Advanced Technology, Chinese Academy of Sciences, Shenzhen, 518055, China(e-mail: w.feng@siat.ac.cn).

injection

Set

$\mathcal{E}_{\text{B}}$	The set of edges in buildings connection
$\mathcal{E}_{\text{IACs}}$	The set of edges in IACs connection
$\mathcal{G}_{\text{B}}$	The buildings topology
$\mathcal{G}_{\text{IACs}}$	The IACs topology
$\mathcal{I}$	The set of buildings
$\mathcal{J}$	The set of rooms in the building
$\mathcal{V}_{\text{B}}$	The set of building nodes
$\mathcal{V}_{\text{IACs}}$	The set of IAC nodes
$\mathbf{s}$	The set of IAC states

Variable

β_i	The building consensus algorithm parameter
$\Delta\theta_i$	The phase angle variation at building i in the system
ΔP^i_{dist}	The active power variation at building i
$\Delta P^i_{\text{Loads}}$	The active power variation of demand-side loads
$\Delta P^i_{\text{noreg}}$	The active power variation of non-regulating loads
ΔP^i_{PVs}	The active power variation of PV power generations
ΔP^i_{reg}	The active power variation of regulation resources
$\Delta Q^i_{\text{Loads}}$	The reactive power variation of demand-side loads
$\Delta Q^i_{\text{noreg}}$	The reactive power variation of non-regulating loads
ΔQ^i_{PVs}	The reactive power variation of PV power generations
ΔQ^i_{reg}	The reactive power variation of regulation resources
ΔV_i	The voltage variation at building i in the system
$\delta_{ij,\widetilde{ij}}$	The IAC consensus algorithm parameter
ΔQ^i_{dist}	The reactive power variation at building i
f^{ij}_{IAC}	The operating frequency of IAC in room j, building i
i	The building number
j	The room number
P^i_{IACs}	The total IACs' active power of building i
Q^i_{IACs}	The total IACs' reactive power of building i
t	The system operating time
$\mathbf{Q}_i$	The control coefficient matrix
$\mathbf{X}_i$	The system state matrix of building i
H^{ij}_{IAC}	The cooling capacity of the IAC in room j, building i
P^{ij}_{IAC}	The active power of IAC in room j, building i
Q^{ij}_{IAC}	The reactive power of IAC in room j, building i
r^i_{p}	The active power regulation signals
r^i_{q}	The reactive power regulation signals
s_{ij}	The IAC operating state
T^{ij}_{in}	The room's indoor temperature in room j, building i
T^{ij}_{o}	The room's outdoor temperature in room j, building i
x_i	The system state of building i
$\mathbf{u}_i$	The control input matrix

I. Introduction

DISTRIBUTION systems face more and more challenges with the increasing share of renewable energy sources (RESs) [1]. One of the key parameters in the stable operation of a distribution system is voltage [2]. RESs, like photovoltaic (PV), are sensitive to ambient conditions and cause many voltage violation problems in distribution systems [3]. For example, the under-voltage problem will occur when there is cloud obstruction on PV panels [4]. Therefore, the voltage violation problem is important in distribution systems with a high penetration of RESs [5]. Since RESs have significant intermittency and uncertainty, traditional voltage regulation methods may be unable to solve voltage problems quickly and effectively [6].

The Internet of Things (IoT) technologies are constantly evolving and gradually being applied to power systems [7]. Based on IoT, demand response [8] is proposed to balance power generation and consumption by changing the operating state of the flexible loads (*e.g.* air conditioners [9], electric vehicle chargers [10], *et al.*). Xie *et al.* [11] propose a two-stage voltage regulation technique for flexible loads to provide voltage regulation services to the distribution systems. Among the various flexible loads, inverter air conditioners (IACs), the common appliances in every house, have the most potential for demand-side loads [12]. Large-scale IACs have been proven effective for providing regulation capacities to distribution systems [13]. Hua *et al.* [14] develop a collaborative voltage regulation algorithm considering the aggregated IACs participation priority for distribution systems. Furthermore, Hua *et al.* [15] demonstrate that IACs can be used as storage battery models to provide voltage auxiliary services to distribution systems.

The above research has used centralized control strategies, while distributed consensus-based control algorithms [16] are increasingly being employed to achieve more efficient and intelligent collaboration among IACs [17]. Wang *et al.* [18] propose a two-layer consensus-based control approach for IACs to mitigate the fluctuations from RESs. However, they do not consider the physical constraints of IACs, which may lead to demand response failures and customer discomfort. Hong *et al.* [19] design a consensus-based control method of large-scale IACs for providing operating reserves considering IACs' physical constraints and thermal comfort for customers. However, the above time-triggered consensus-based control approaches have high requirements for communication. To enhance the efficiency of IAC control, many scholars have incorporated event-triggered mechanisms into consensus-based algorithms to alleviate the communication burden. Zhao *et al.* [20] propose a distributed event-triggered consensus-based control strategy for the IACs and other regulation resources to participate in frequency regulation. The above research has demonstrated that distributed consensus-based control algorithms have better data privacy protection, less communication, and comfort guarantee [21].

Another issue worth mentioning is that most researchers only consider the active power of the IACs to provide auxiliary regulation services to the distribution system. These studies only model the active power of IACs, with reactive power varying in tandem with active power. The lack of purposeful inclusion of reactive power in the control process will lead to insufficient accuracy in voltage control. Therefore, reactive power compensation is also crucial in maintaining the system voltage within a security range in the distribution system. Zhu *et al.* [22] provide a hierarchical framework that coordinates voltage control between transmission and distribution systems using inverter-based resources. Hu *et al.* [23] propose a control strategy for the reactive power compensation ability of electric vehicle chargers and integrate this inverter-based resource into real-time distribution system voltage regulation. The above

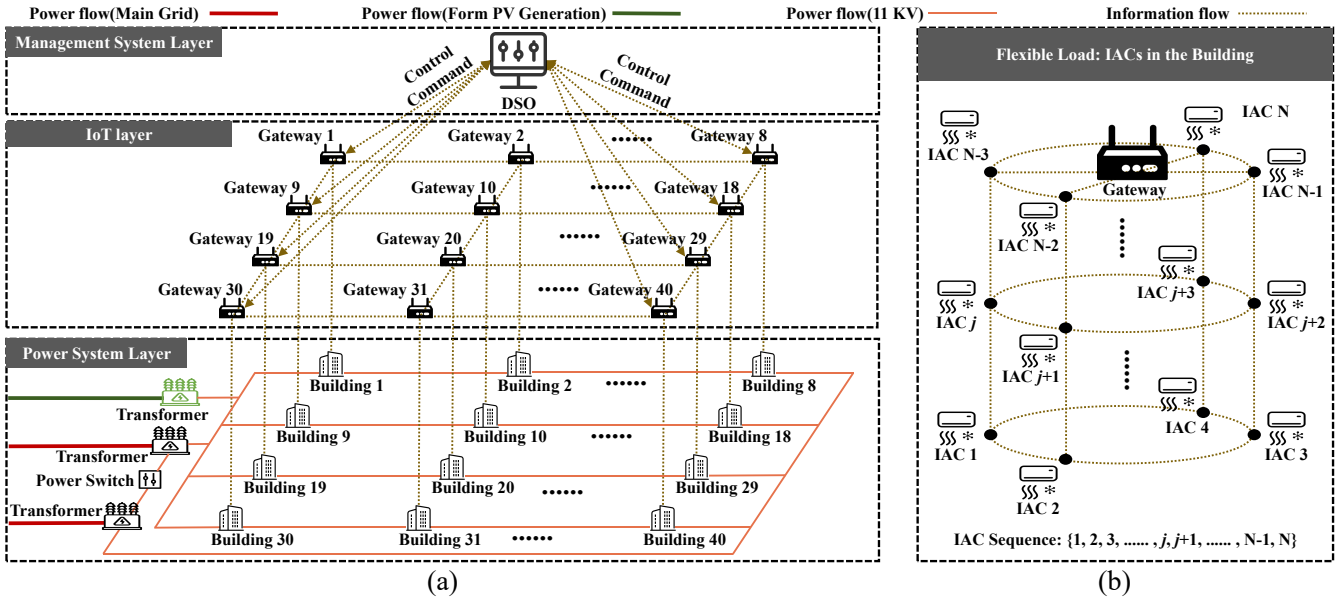

Fig. 1. (a) A typical distribution system structure with large-scale aggregated IACs; (b) IACs are aggregated by the IoT gateway in the building.

research shows that the reactive power of inverter-based resources can also be used to provide voltage regulation services. Viriyautsahakul *et al.* [24] analyze the IACs' inverter and converter design and show that IAC can provide reactive power to power systems. This study demonstrates that the reactive power of IACs can also be utilized for voltage regulation in distribution systems. Therefore, it is necessary to design an efficient method to coordinate the active and reactive power of the IAC to participate in voltage regulation.

Model Predictive Control (MPC) can be utilized to coordinate the active and reactive power of IAC. MPC can convert control problems into optimization problems and obtain the optimal control strategy for IACs. Zhao *et al.* [25] propose an IAC control method based on MPC for frequency control considering communication delay. However, this method still uses centralized control strategies. Some scholars have utilized distributed mind-setting to solve the optimal problems of MPC [26]. Zhang *et al.* [27] propose a distributed model predictive control based coordinated control method for the voltage security of the integrated hybrid energy system. This research shows that distributed model predictive control allows collaboration on regulation goals with a partial exchange of information. However, this research does not achieve thermal comfort for customers during the regulation process. Thermal comfort is a significant factor influencing whether or not customers participate in demand response [28]. Therefore, thermal comfort should also be considered during voltage regulation. More significantly, most MPC studies mentioned above do not consider the coordination of the active and reactive power of IACs.

To fill the above research gaps, this paper proposes a distributed consensus-based MPC (DCMPC) algorithm aiming to coordinate the active and reactive power of IACs to participate in voltage regulation. DCMPC combines the principles of distributed control with the solution of optimal control sequences. The main contributions are as follows:

- A comprehensive voltage regulation model coordinating both active and reactive power of IACs. Existing research only considers active power of IACs while the reactive power passively follows the active power. Therefore, the coupling characteristics of IACs' active and reactive power are explicitly integrated into the voltage regulation process in this research. Furthermore, the thermal comfort constraint is dynamically embedded into the regulation model to maintain customer comfort.
- A DCMPC framework is proposed to coordinate large-scale IACs. Building upon our previous centralized MPC study [29], this paper advances to a distributed architecture. Through distributed information exchange among adjacent buildings, the distribution system voltage regulation can be achieved in a fast and scalable way. The consensus mechanism enables each IAC to adjust its operating state according to control signals and indoor temperature, thereby satisfying the heterogeneous comfort requirements. Meanwhile, the MPC framework employs rolling optimization to predict future voltages and calculate control inputs, ensuring both voltage security and room comfort.
- A hardware-in-the-loop (HIL) experiment platform with Real-Time Digital Simulator (RTDS) and IoT-based IACs management system is developed to verify the proposed DCMPC algorithm. IoT-based IACs management system allows the realistic IACs to provide voltage regulation services to distribution systems.

The remainder of this paper is organized as follows. Section II models the voltage regulation problem. Section III proposes the DCMPC-based voltage regulation method. Section IV describes the HIL platform. Section V illustrates the experiments and analyzes the results of the experiments. Section VI concludes this paper.

II. System Formulation

A. System Structure

Fig. 1(a) shows a typical distribution system structure with flexible loads to address the voltage fluctuations. The system can be divided into three layers: the management layer with

the distribution system operator (DSO), the IoT layer with the gateway, and the power system layer with the distribution system. The distribution system based on a campus with 40 buildings is adopted in this research. DSO monitors the operation status of the distribution system and ensures that the voltage of 40 buildings is within the security range. Fig. 1(b) shows the flexible load (i.e., IAC) in the building. Each building's IACs are aggregated through the IoT gateway and finally enabled to transmit status data to the DSO and receive control commands from the DSO.

B. Modeling of Inverter Air Conditioners

The operation of IACs and the thermodynamic process of the corresponding rooms can be expressed based on the ETP model [30]. The thermodynamic process of the room considering the indoor temperature can be expressed as follows:

$$C_{\text{room}}^{ij}\frac{\mathrm{d}T_{\text{in}}^{ij}(t)}{\mathrm{d}t}=\frac{T_{\text{o}}^{ij}(t)-T_{\text{in}}^{ij}(t)}{R_{\text{room}}^{ij}}-H_{\text{IAC}}^{ij}(t), \tag{1}$$

where C_{room}^{ij} is the room's equivalent air heat capacity; R_{room}^{ij} is the equivalent thermal resistance of the room's envelope; $T_{\text{in}}^{ij}(t)$ is the room's indoor temperature at time t; $T_{\text{o}}^{ij}(t)$ is the room's outdoor temperature at time t; $H_{\text{IAC}}^{ij}(t)$ is the cooling capacity of the IAC at time t; i is the building number, $\forall i \in \mathcal{I}$; $\mathcal{I}=\{1,2,3,...,M\}$ is the set of buildings; M is the total building number in the distribution system; j is the room number, $\forall j \in \mathcal{J}$; $\mathcal{J}=\{1,2,3,...,N\}$ is the set of rooms; N is the total room number in a building.

The IAC's operating power and cooling capacity are primarily determined by its compressor's operating frequency [31]. Kim *et al.* [32] establish a simplified linear model for the IAC compressor's power and frequency linear relationship and verify the model through experiments. The model reduces the computational burden and has been widely integrated into many control research studies [33]. In this study, this linear model for IACs is adopted, which is expressed as follows:

$$\begin{cases} P_{\text{IAC}}^{ij}(t)=\kappa_1^{ij}f_{\text{IAC}}^{ij}(t)+b_1^{ij}, \\ H_{\text{IAC}}^{ij}(t)=\kappa_2^{ij}f_{\text{IAC}}^{ij}(t)+b_2^{ij}, \end{cases} \tag{2}$$

where κ_1^{ij} and b_1^{ij} are the coefficients of the IAC's operating power; κ_2^{ij} and b_2^{ij} are the coefficients of the IAC's cooling capacity; $P_{\text{IAC}}^{ij}(t)$ and $f_{\text{IAC}}^{ij}(t)$ are the compressor's operating active power and operating frequency of IAC at time t, respectively. In this research, we are mainly concerned with utilizing the IAC's power (i.e., active and reactive power) to realize the voltage regulation objective by reducing the IAC's power consumption. Particularly, we consider the reactive power variations during voltage regulation which is not a concern in previous research on IAC participation in voltage control. Reactive power is determined by active power and phase deviation between the voltage and current of the IAC [34], which can be expressed as follows:

$$Q_{\text{IAC}}^{ij}(t)=P_{\text{IAC}}^{ij}(t)\tan\phi^{ij}, \tag{3}$$

where Q_{IAC}^{ij} is the reactive power of the IAC; ϕ^{ij} is the phase deviation between the voltage and current of the IAC; $\tan\phi^{ij}$ is the tangent value of the phase deviation ϕ^{ij}. The power factor, defined as $\cos\phi^{ij}$, indicates the impact of the phase deviation on the energy utilization efficiency of the IAC. Since the room parameters (C_{room}^{ij}, R_{room}^{ij}) and the IAC parameters (κ_1^{ij},κ_2^{ij},b_1^{ij},b_2^{ij}) are regarded to be fixed, the active and reactive power consumption of the IAC at time t can be expressed as follows:

$$\begin{cases} P_{\text{IAC}}^{ij}(t)=\text{f}_{\text{P}}(f_{\text{IAC}}^{ij}(t),T_{\text{o}}^{ij}(t),T_{\text{in}}^{ij}(t)), \\ Q_{\text{IAC}}^{ij}(t)=\text{f}_{\text{Q}}(f_{\text{IAC}}^{ij}(t),T_{\text{o}}^{ij}(t),T_{\text{in}}^{ij}(t),\cos\phi(t)). \end{cases} \tag{4}$$

The above equations provide the active and reactive power consumption of the single IAC at time t. However, the regulation capacity of a single IAC is relatively small (at the kW and $kVar$ level). Aggregating multiple IACs can obtain significant regulation capacity [35]. The regulation capacity of aggregating multiple IACs in building i at time t can be expressed as follows:

$$\begin{cases} P_{\text{IACs}}^{i}(t)=\sum\limits_{j=1}^{N}P_{\text{IAC}}^{ij}(t), \\ Q_{\text{IACs}}^{i}(t)=\sum\limits_{j=1}^{N}Q_{\text{IAC}}^{ij}(t), \end{cases} \tag{5}$$

where $P_{\text{IACs}}^{i}(t)$ is the total IACs' active power of building i; $Q_{\text{IACs}}^{i}(t)$ is the total IACs' reactive power of building i.

C. Modeling of the Distributed System

The voltage variation at each node is influenced by power generation and consumption. The node voltage and power injection of the distribution system can be expressed as follows:

$$\begin{bmatrix} \Delta\theta \\ \Delta\mathbf{V} \end{bmatrix}=\mathbf{J}^{-1}\begin{bmatrix} \Delta\mathbf{P}_{\text{dist}} \\ \Delta\mathbf{Q}_{\text{dist}} \end{bmatrix}=\begin{bmatrix} \mathbf{S}_{\text{P}\theta} & \mathbf{S}_{\text{Q}\theta} \\ \mathbf{S}_{\text{PU}} & \mathbf{S}_{\text{QU}} \end{bmatrix}\begin{bmatrix} \Delta\mathbf{P}_{\text{dist}} \\ \Delta\mathbf{Q}_{\text{dist}} \end{bmatrix}, \tag{6}$$

where $\Delta\theta$ is the variation of phase angle at each node in the system, $\Delta\theta = [\ \theta_1(t)\ ...\ \theta_i(t)\ ...\ \theta_M(t)\ ]^{\text{T}}$; $\Delta\mathbf{V}$ is the variation of voltage at each node in the system, $\Delta\mathbf{V} = [\ V_1(t)\ ...\ V_i(t)\ ...\ V_M(t)\ ]^{\text{T}}$; $\Delta\mathbf{P}_{\text{dist}}$ and $\Delta\mathbf{Q}_{\text{dist}}$ are the active and reactive power variation at each node, respectively. $\Delta\mathbf{P}_{\text{dist}} = [\ P_{\text{dist}}^{1}(t)\ ...\ P_{\text{dist}}^{i}(t)\ ...\ P_{\text{dist}}^{M}(t)\ ]^{\text{T}}$ and $\Delta\mathbf{Q}_{\text{dist}} = [\ Q_{\text{dist}}^{1}(t)\ ...\ Q_{\text{dist}}^{i}(t)\ ...\ Q_{\text{dist}}^{M}(t)\ ]^{\text{T}}$. $\mathbf{J}$ is the jacobian matrix with a dimension of $2M \times 2M$. It depends on both the distribution system topology and the current operating point [36]. In this study, the Jacobian matrix $\mathbf{J}$ is evaluated at each operating point using the voltages, phase angle, and power injection obtained from RTDS simulations. The $\mathbf{J}^{-1}$ in the above equation can be represented by the voltage sensitivity matrix. The voltage sensitivity matrix is consist of four $M \times M$ submatrices $\mathbf{S}_{\text{P}\theta}$, $\mathbf{S}_{\text{Q}\theta}$, $\mathbf{S}_{\text{PU}}$ and $\mathbf{S}_{\text{QU}}$. $\mathbf{S}_{\text{P}\theta}$ and $\mathbf{S}_{\text{Q}\theta}$ are the phase angle sensitivity of active and reactive power, respectively. $\mathbf{S}_{\text{PU}}$ and $\mathbf{S}_{\text{QU}}$ are the voltage sensitivity of active and reactive power, respectively. The voltage sensitivity matrix represents the relationship between node voltages and power injection. The power variation can be expressed as follows:

$$\begin{cases} \Delta P_{\text{dist}}^{i}(t)=\Delta P_{\text{Loads}}^{i}(t)+\Delta P_{\text{PVs}}^{i}(t), \\ \Delta Q_{\text{dist}}^{i}(t)=\Delta Q_{\text{Loads}}^{i}(t)+\Delta Q_{\text{PVs}}^{i}(t), \end{cases} \tag{7}$$

where $\Delta P_{\text{PVs}}^{i}$ and $\Delta Q_{\text{PVs}}^{i}$ are the active and reactive power variation at building i caused by the PV power generation, respectively; $\Delta P_{\text{Loads}}^{i}$ and $\Delta Q_{\text{Loads}}^{i}$ are the active and reactive

power variation at building i caused by the demand-side load, respectively. The demand-side loads consist of two main components: regulation resources, which in this context are IACs, and non-regulating loads. The active and reactive power variation of demand-side loads can be expressed as follows:

$$\begin{cases} \Delta P^i_{\text{Loads}}(t) = \Delta P^i_{\text{reg}}(t) + \Delta P^i_{\text{noreg}}(t), \\ \Delta Q^i_{\text{Loads}}(t) = \Delta Q^i_{\text{reg}}(t) + \Delta Q^i_{\text{noreg}}(t), \\ \Delta P^i_{\text{reg}}(t) = P^i_{\text{IACs}}(t) - P^i_{\text{IACs}}(t-1), \\ \Delta Q^i_{\text{reg}}(t) = Q^i_{\text{IACs}}(t) - Q^i_{\text{IACs}}(t-1), \end{cases} \tag{8}$$

where $\Delta P^i_{\text{noreg}}$ and $\Delta Q^i_{\text{noreg}}$ are the active and reactive power variation of non-regulating loads, respectively; ΔP^i_{reg} and ΔQ^i_{reg} are the active and reactive power variation of the regulation resources, respectively.

The Eq. (6) describes the basic principle of phase angle deviations and voltage deviations in the distribution system. The voltage deviation is related to the deviations of active and reactive power, which can be expressed as follows:

$$\Delta V_i = V_i(t+1) - V_i(t) = \begin{bmatrix} \mathbf{S}^i_{\text{PU}} & \mathbf{S}^i_{\text{QU}} \end{bmatrix} \begin{bmatrix} \Delta \mathbf{P}_{\text{dist}}(\mathbf{t}) \\ \Delta \mathbf{Q}_{\text{dist}}(\mathbf{t}) \end{bmatrix}, \tag{9}$$

where $\mathbf{S}^i_{\text{PU}}$ and $\mathbf{S}^i_{\text{QU}}$ are the i row of $\mathbf{S}_{\text{PU}}$ and $\mathbf{S}_{\text{QU}}$, respectively. The Eq. (9) formulates the voltage deviation ΔV_i at node i as the matrix product of the voltage sensitivity vector and the system power variation vector of the system. To facilitate subsequent calculations, the above equation can be rewritten as follows:

$$x_i(t+1) = x_i(t) + \mathbf{B}_{i,i}\mathbf{u}_i(t) + \sum_{\widetilde{i}=1,\widetilde{i}\neq i}^{M} \mathbf{B}_{i,\widetilde{i}}\mathbf{u}_{\widetilde{i}}(t), \tag{10}$$

where

$$\begin{cases} x_i(t) = V_i(t), \\ \mathbf{B}_{i,i} \triangleq \begin{bmatrix} S^{i,i}_{\text{PU}} & S^{i,i}_{\text{QU}} \end{bmatrix}, \mathbf{B}_{i,\widetilde{i}} \triangleq \begin{bmatrix} S^{i,\widetilde{i}}_{\text{PU}} & S^{i,\widetilde{i}}_{\text{QU}} \end{bmatrix}, \\ \mathbf{u}_i(t) \triangleq \begin{bmatrix} \Delta P^i_{\text{dist}}(t) \\ \Delta Q^i_{\text{dist}}(t) \end{bmatrix}, \mathbf{u}_{\widetilde{i}}(t) \triangleq \begin{bmatrix} \Delta P^{\widetilde{i}}_{\text{dist}}(t) \\ \Delta Q^{\widetilde{i}}_{\text{dist}}(t) \end{bmatrix}, \end{cases} \tag{11}$$

where $\forall \widetilde{i} \in \mathcal{I}$; $S^{i,i}_{\text{PU}}$ and $S^{i,i}_{\text{QU}}$ are the voltage sensitivity of building i active and reactive power injection, respectively; $S^{i,\widetilde{i}}_{\text{PU}}$ and $S^{i,\widetilde{i}}_{\text{QU}}$ are the voltage sensitivity of active and reactive power injection from building i to its neighboring building $\widetilde{i}$, respectively; $\mathbf{u}_i$ and $\mathbf{u}_{\widetilde{i}}$ are the control input matrix. In this rewritten form, the original voltage sensitivity vector is expanded into $\mathbf{B}_{i,i}$ and $\mathbf{B}_{i,\widetilde{i}}$, while the system power variation vector is expanded into $\mathbf{u}_i$ and $\mathbf{u}_{\widetilde{i}}$.

D. Modeling of Communication Topology

An accurate topology is critical to design the cost function in the distributed voltage regulation. As shown in Fig. 1(a), the DSO only communicates with IoT gateways in buildings close to the transformer in the distribution system. The adjacent IoT gateways in the building are allowed to communicate. The IACs in each building are aggregated through the IoT gateways. The adjacent IACs in the building are allowed to communicate. Therefore, there are IACs topology $\mathcal{G}_{\text{IACs}} = \{\mathcal{V}_{\text{IACs}}, \mathcal{E}_{\text{IACs}}\}$ and buildings topology $\mathcal{G}_{\text{B}} = \{\mathcal{V}_{\text{B}}, \mathcal{E}_{\text{B}}\}$ in this study; where $\mathcal{V}_{\text{IACs}}$ is the set of IAC nodes; $\mathcal{V}_{\text{B}}$ is the set of building nodes; $\mathcal{E}_{\text{IACs}} \subseteq \mathcal{V}_{\text{IACs}} \times \mathcal{V}_{\text{IACs}}$ is the set of edges in IACs connection; $\mathcal{E}_{\text{B}} \subseteq \mathcal{V}_{\text{B}} \times \mathcal{V}_{\text{B}}$ is the set of edges in buildings connection. The relationship among the nodes in the communication topology is defined as follows:

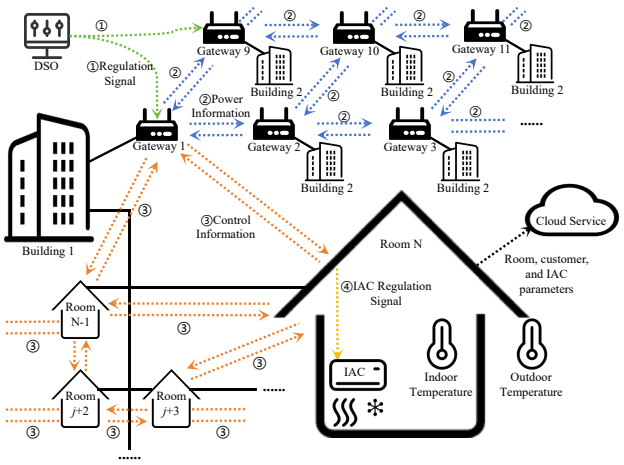

Fig. 2. The structure of the DCMPC.

$$\begin{cases} a_{ij,\widetilde{ij}} = 1, if\{ij,\widetilde{ij}\} \in \mathcal{E}_{\text{IACs}}, \\ a_{ij,\widetilde{ij}} = 0, if\{ij,\widetilde{ij}\} \notin \mathcal{E}_{\text{IACs}}, \\ \gamma_{i,\widetilde{i}} = 1, if\{i,\widetilde{i}\} \in \mathcal{E}_{\text{B}}, \\ \gamma_{i,\widetilde{i}} = 0, if\{i,\widetilde{i}\} \notin \mathcal{E}_{\text{B}}, \end{cases} \tag{12}$$

where $\forall \widetilde{i} \in \mathcal{I}$; $\forall \widetilde{j} \in \mathcal{J}$; $\{ij,\widetilde{ij}\}$ means that there is an undirectional edge between IAC (ij) and IAC $(\widetilde{ij})$ in the graph; $\{i,\widetilde{i}\}$ means that there is an undirectional edge between building i and building $\widetilde{i}$ in the graph.

III. Design of Distributed Consensus-Based MPC Method

A. Structure of the DCMPC

This paper proposes the DCMPC method to coordinate the active and reactive power of IACs to participate in voltage regulation and achieve thermal comfort for customers during voltage regulation. The structure of the proposed DCMPC algorithm is shown in Fig. 2 and the pseudo-code is shown in Algorithm 1. In this study, the IoT gateway plays an important role in facilitating the transmission of control signals between the DSO and specific buildings, while managing the power regulation of IACs within each building. The DSO will send regulation signals directly to specific buildings $(1, 9, ...)$, which are adjacent to the DSO as shown in Fig. 2. These specific buildings change the operating power of the IACs in response to regulation signals. And the neighbouring buildings $(2, 10, ...)$ will also adjust their IACs' operating status according to the state of the specific buildings. For each building, the IACs control signals are sent down through the IoT gateway. Due to the large number of IACs in the building, the IoT gateway will only transmit control signals directly to specific IACs. As shown in Fig. 2, the IoT gateway in building 1 will send the control signals directly to specific IACs $(N-1, N, ...)$. Other IACs in the building interact with neighbouring IACs through the communications network. Finally, the whole building cooperates to complete the optimal control action. This process is also referred to as distributed

Algorithm 1: Distributed Consensus-Based Model Predictive Control (DCMPC) Algorithm

Input: Initialisation Value: Room parameters:$(C^{ij}_{\text{room}}, R^{ij}_{\text{room}}, T^{ij}_{\text{in}}, T^{ij}_{\text{o}})$ of each room; IAC parameters: $(\kappa^{ij}_1, b^{ij}_1, \kappa^{ij}_2, b^{ij}_2, \overline{f^{ij}_{\text{IAC}}(t)}, \underline{f^{ij}_{\text{IAC}}(t)}, f^{ij}_{\text{ref}}(t))$ of each IAC; Power System to RTDS: $(P^i_{\text{Loads}}, Q^i_{\text{Loads}}, P^i_{\text{PVs}}, Q^i_{\text{PVs}})$ of each node; Comfort temperature range of the customer: $[T^{ij}_{\min}, T^{ij}_{\max}]$;

Update: Node voltage V_i; Room indoor temperature T^{ij}_{in}; IACs power $P^{ij}_{\text{IAC}}(t)$ and $Q^{ij}_{\text{IAC}}(t)$ of each building.

Obtain RTDS node status $(P^i_{\text{Loads}}, Q^i_{\text{Loads}}, P^i_{\text{PVs}}, Q^i_{\text{PVs}}, V_i)$;

if *PCC voltage V_0 does not exceed the setting threshold of* $[0.95, 1.05]p.u.$ **then**

  Return.

else

  DSO sends the control signal to the $(1, 8, 9, 18, 19, 29, 30, 40)$ IoT gateway;

  for $i = 1, 2, ..., 40$ **do**

    STEP1: Construct the state equation $x_i(t)$ based on physical description of the distribution system according to **Eq.10**;

    STEP2: Construct the predictive model $\mathbf{X}_i(t)$ in the building according to **Eqs.13-16**;

    STEP3: Solve the optimal problem(**Eqs. 24-26**) to obtain the control input $\mathbf{u}^{\text{o}(1)}_i(\Delta P^i_{\text{IACs}}\ and\ \Delta Q^i_{\text{IACs}})$ of IACs;

    STEP4: **if** *IACs control event determination:* $c_i(t) = 1$*(Based on **Eq.23**)* **then**

      STEP5: IoT gateway update the state(active power regulation signals $r^i_{\text{p}}(t)$ and reactive power regulation signals $r^i_{\text{q}}(t)$) base on consensus process **Eq.22**;

      STEP6: Calculate the IAC state s_{ij} base on consensus process **Eqs.18-21**:

      if $T^{ij}_{\text{IAC}}(t) \in [T^{ij}_{\min}, T^{ij}_{\max}]$ **then**

        IAC changes state $s_{ij}(t)$, the compressor frequency$f^{ij}_{\text{IAC}}(t)$ update;

      else

        IAC without regulation, the $s_{ij}(t)$ and $f^{ij}_{\text{IAC}}(t)$ do not change;

      STEP7: Calculate the power $P^{ij}_{\text{IAC}}(t)$ and $Q^{ij}_{\text{IAC}}(t)$ of each IACs according to **EqS.1-4**;

      STEP8: Calculate the power $P^i_{\text{IACs}}(t)$ and $Q^i_{\text{IACs}}(t)$ of IACs for each building according to **Eq.5**.

Update the IACs power $P^i_{\text{IACs}}(t)$ and $Q^i_{\text{IACs}}(t)$ to RTDS node status $(P^i_{\text{Loads}}, Q^i_{\text{Loads}})$.

consensus control. DCMPC is fundamentally based on the traditional MPC and integrates the distributed consensus control. The consensus-based approach ensures that control strategies among buildings remain consistent through collaboration.

B. Predictive Model

Eq.(10) provides the physical description of the distribution system. It reflects the coupling between the voltage and the active and reactive power injection of all nodes. In the DCMPC framework, the predictive model of building i from the moment t to the moment $t+p$ can be expressed as follows:

$$\begin{cases} x_i(t+1|t) = & x_i(t) + \mathbf{B}_{i,i}\mathbf{u}_i(t|t) + \sum\limits_{\widetilde{i}=1,\widetilde{i}\neq i}^{M} \mathbf{B}_{i,\widetilde{i}}\mathbf{u}_{\widetilde{i}}(t|t), \\ x_i(t+2|t) = & x_i(t) + \mathbf{B}_{i,i}\sum\limits_{k=0}^{1}\mathbf{u}_i(t+k|t) + \\ & \sum\limits_{\widetilde{i}=1,\widetilde{i}\neq i}^{M}\mathbf{B}_{i,\widetilde{i}}\sum\limits_{k=0}^{1}\mathbf{u}_{\widetilde{i}}(t+k|t), \\ & \cdots\cdots, \\ x_i(t+p|t) = & x_i(t+1) + \mathbf{B}_{i,i}\sum\limits_{k=0}^{p-1}\mathbf{u}_i(t+k|t) + \\ & \sum\limits_{\widetilde{i}=1,\widetilde{i}\neq i}^{M}\mathbf{B}_{i,\widetilde{i}}\sum\limits_{k=0}^{p-1}\mathbf{u}_{\widetilde{i}}(t+k|t), \end{cases} \tag{13}$$

where $\mathbf{u}_i(t+p|t)$ denote the predicted control input of the step $t+p$ at moment t; $\mathbf{x}_i(t+p|t)$ denote the predicted system state of the step $t+p$ at moment t. For calculation purposes, Eq. (13) can be simplified as follows:

$$\mathbf{X}_i(t) = x_i(t) + \mathbf{G}_i\mathbf{U}_i(t) + \sum_{\widetilde{i}=1,\widetilde{i}\neq i}^{M}\mathbf{G}_{\widetilde{i}}\mathbf{U}_{\widetilde{i}}(t)), \tag{14}$$

where

$$\begin{aligned} \mathbf{X}_i(t) &= \begin{bmatrix} x_i(t+1|t) & x_i(t+2|t) & \dots & x_i(t+p|t) \end{bmatrix}^{\text{T}}, \\ \mathbf{U}_i(t) &= \begin{bmatrix} \mathbf{u}_i(t|t) & \mathbf{u}_i(t+1|t) & \dots & \mathbf{u}_i(t+p-1|t) \end{bmatrix}^{\text{T}}, \\ \mathbf{U}_{\widetilde{i}}(t) &= \begin{bmatrix} \mathbf{u}_{\widetilde{i}}(t|t) & \mathbf{u}_{\widetilde{i}}(t+1|t) & \dots & \mathbf{u}_{\widetilde{i}}(t+p-1|t) \end{bmatrix}^{\text{T}}, \end{aligned} \tag{15}$$

$$\mathbf{G}_i = \begin{bmatrix} \mathbf{B}_{i,i} & 0 & \dots & 0 \\ \dots & \dots & \dots & 0 \\ \mathbf{B}_{i,i} & \mathbf{B}_{i,i} & \dots & 0 \\ \dots & \dots & \dots & \dots \\ \mathbf{B}_{i,i} & \mathbf{B}_{i,i} & \dots & \mathbf{B}_{i,i} \end{bmatrix}, \mathbf{G}_{\widetilde{i}} = \begin{bmatrix} \mathbf{B}_{i,\widetilde{i}} & 0 & \dots & 0 \\ \dots & \dots & \dots & 0 \\ \mathbf{B}_{i,\widetilde{i}} & \mathbf{B}_{i,\widetilde{i}} & \dots & 0 \\ \dots & \dots & \dots & \dots \\ \mathbf{B}_{i,\widetilde{i}} & \mathbf{B}_{i,\widetilde{i}} & \dots & \mathbf{B}_{i,\widetilde{i}} \end{bmatrix}. \tag{16}$$

C. Model Constraints

The prediction model is mainly constrained by the operating limitations of distribution systems and IACs. To ensure the voltage security of distribution systems, the fluctuation range of the voltage is limited to $[0.95, 1.05]$ $p.u.$, which can be expressed as follows:

$$0.95 \leq \frac{x_i(t)}{V^{\text{ref}}_i} \leq 1.05. \tag{17}$$

The constraints of the IAC include the operating power constraint and thermal comfort constraint.

a) The IAC operating power constraint: The active power output P_{IAC}^{ij} and reactive power output Q_{IAC}^{ij} of the IAC must operate within their rated capacities. These constraints ensure that the control input operates within the practical operational range of the IAC.

b) The thermal comfort constraint: As shown in Fig. 3, the indoor temperature $T_{\mathrm{in}}^{ij}(t)$ needs to stay within the customer comfort requirement, thereby achieving thermal comfort. The DSO can send messages to the building's IoT gateway to adjust the IAC's power up and down. If the indoor temperature does not reach the down regulation temperature limit $T_{\max}^{ij}$, the IAC can switch to down regulation. Alternatively, if the indoor temperature does not reach the up regulation temperature limit $T_{\min}^{ij}$, the IAC can switch to up regulation. If the temperature exceeds the customer comfort requirement, the IAC operates in stop regulation state. The above constraints of the IAC can be expressed as follows:

$$\begin{cases} 0 \le P_{\mathrm{IAC}}^{ij} \le P_{\mathrm{IAC,max}}^{ij}, \\ 0 \le Q_{\mathrm{IAC}}^{ij} \le Q_{\mathrm{IAC,max}}^{ij}, \\ T_{\min}^{ij} \le T_{\mathrm{in}}^{ij}(t) \le T_{\max}^{ij}, \end{cases} \tag{18}$$

where $P_{\mathrm{IAC,max}}^{ij}$ and $Q_{\mathrm{IAC,max}}^{ij}$ are the rated active and reactive power of the IAC, respectively; $T_{\mathrm{in}}^{ij}(t)$ is the indoor temperature at time t, $T_{\min}^{ij}$ and $T_{\max}^{ij}$ are the minimum and maximum allowable temperatures, respectively.

D. IACs State Definition

The active and reactive power of the IAC depends on the operating state $s_{ij}(t)$. The state is determined by both the IAC and the indoor temperature. The DSO can control the state of the IAC by sending status messages to the building's IoT gateway. In this way, the customer's privacy can also be effectively protected. The IACs' states $\mathbf{s} = [s_{11}, s_{12}, ...s_{ij}, ...s_{MN}]$, are defined as follows:

$$s_{ij}(t) = \begin{cases} \frac{f_{\mathrm{IAC}}^{ij}(t) - f_{\mathrm{ref}}^{ij}}{\overline{f_{\mathrm{IAC}}^{ij}} - f_{\mathrm{ref}}^{ij}}, & Up\ Reg.\ and \\ & T_{\mathrm{in}}^{ij}(t) \in [T_{\min}^{ij}, T_{\max}^{ij}], \\ \frac{f_{\mathrm{IAC}}^{ij}(t) - f_{\mathrm{ref}}^{ij}}{\underline{f_{\mathrm{IAC}}^{ij}} - f_{\mathrm{ref}}^{ij}}, & Down\ Reg.\ and \\ & T_{\mathrm{in}}^{ij}(t) \in [T_{\min}^{ij}, T_{\max}^{ij}], \\ s_{ij}(t), & Stop\ Reg.\ or \\ & T_{\mathrm{in}}^{ij}(t) \notin [T_{\min}^{ij}, T_{\max}^{ij}], \end{cases} \tag{19}$$

where f_{ref}^{ij} is the initial operating frequency of the IAC in room j, building i; $\overline{f_{\mathrm{IAC}}^{ij}}$ is the upper limitation of the IAC's operating frequency; $\underline{f_{\mathrm{IAC}}^{ij}}$ is the lower limitation of the IAC's operating frequency; $\overline{f_{\mathrm{IAC}}^{ij}}$ and $\underline{f_{\mathrm{IAC}}^{ij}}$ are subject to device features. f_{IAC}^{ij} is the operating frequency of the IAC in room j, building i which is defined as follows:

$$f_{\mathrm{IAC}}^{ij}(t) = \begin{cases} f_{\mathrm{ref}}^{ij} - s_{ij}(t)(f_{\mathrm{ref}}^{ij} - \overline{f_{\mathrm{IAC}}^{ij}}), & Up\ Reg.\ and \\ & T_{\mathrm{in}}^{ij}(t) \in [T_{\min}^{ij}, T_{\max}^{ij}], \\ f_{\mathrm{ref}}^{ij} - s_{ij}(t)(f_{\mathrm{ref}}^{ij} - \underline{f_{\mathrm{IAC}}^{ij}}), & Down\ Reg.\ and \\ & T_{\mathrm{in}}^{ij}(t) \in [T_{\min}^{ij}, T_{\max}^{ij}], \\ f_{\mathrm{ref}}^{ij}, & Stop\ Reg.\ or \\ & T_{\mathrm{in}}^{ij}(t) \notin [T_{\min}^{ij}, T_{\max}^{ij}] \end{cases} \tag{20}$$

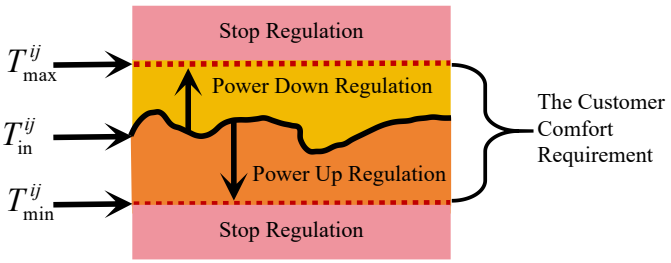

Fig. 3. The thermal comfort constraint of the IAC.

E. Consensus Algorithm of IACs

The state of the IAC in the building is changed by interacting control information with neighbouring IACs. The consensus-based approach ensures that control strategies among IACs in the system remain consistent. According to the standard average consensus algorithm for the undirected graph [37], the relationship among the nodes of the IACs can be expressed as follows:

$$\dot{s_{i\widetilde{j}}}(t) = \sum_{j=1, j\neq\widetilde{j}}^{N} \delta_{ij,i\widetilde{j}} a_{ij,i\widetilde{j}} (s_{ij}(t) - s_{i\widetilde{j}}(t)), \tag{21}$$

where $\delta_{ij,i\widetilde{j}}$ denotes the coupling strength between node j and node $\widetilde{j}$ in building i. The consensus algorithm parameter $\delta_{ij,i\widetilde{j}}$ mainly affects the speed and range of regulation among neighboring IACs. Higher values indicate faster regulation, while lower values indicate slower regulation. Through the above information interaction process, the IACs in the building can finally realise the regulation signals of the IoT gateway. The IoT gateway states of the building i, i.e., the active power regulation signals $r_{\mathrm{p}}^{i}(t)$ and reactive power regulation signals $r_{\mathrm{q}}^{i}(t)$, can be expressed as follows:

$$\begin{cases} \dot{r_{\mathrm{p}}}(t) = c_i(t)[\sum_{j=1}^{N} a_{ij,i_r j_r}(s_{ij}(t) - r_{\mathrm{p}}^{i}(t)) + \beta_i \Delta P_{\mathrm{IACs}}^{i}], \\ \dot{r_{\mathrm{q}}}(t) = c_i(t)[\sum_{j=1}^{N} a_{ij,i_r j_r}(s_{ij}(t) - r_{\mathrm{q}}^{i}(t)) + \beta_i \Delta Q_{\mathrm{IACs}}^{i}], \end{cases} \tag{22}$$

where $c_i(t)$ is the event trigger function, which determines whether the IoT gateway sends the regulation signal or not; $i_r j_r$ is the node number of the IoT gateway in the building. $a_{ij,i_r j_r}$ denotes the relationship between IACs ij and IoT gateway. The $a_{ij,i_r j_r}$ is 1 if there is communication between IAC ij and IoT gateway, otherwise the $a_{ij,i_r j_r}$ is 0. β_i is the control coefficient of the active and reactive power regulation signal; β_i determines how fast or slow the IoT gateway sends power regulation signals to the IAC ij. Higher weights indicate faster regulation, while lower weights indicate slower regulation. $c_i(t)$ can be expressed as follows:

$$c_i(t) = \begin{cases} 1, & |\Delta P_{\mathrm{IACs}}^{i}| > P_{\mathrm{thr}}^{i} \quad or \quad |\Delta Q_{\mathrm{IACs}}^{i}| > Q_{\mathrm{thr}}^{i}, \\ 0, & otherwise, \end{cases} \tag{23}$$

where P_{thr}^{i} and Q_{thr}^{i} are the active and reactive power variation limitation of the building i, respectively.

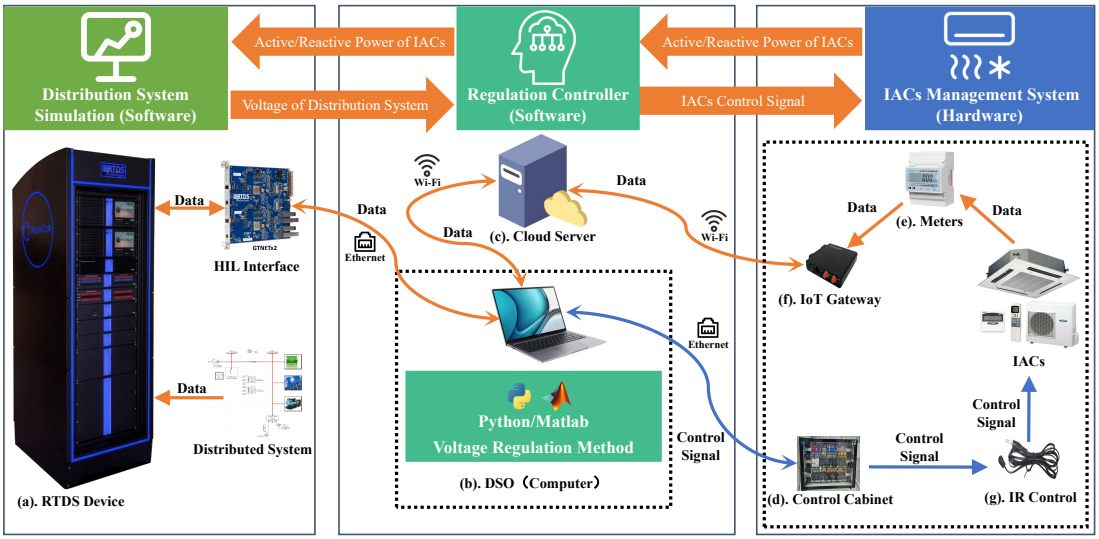

Fig. 4. The structure of HIL platform.

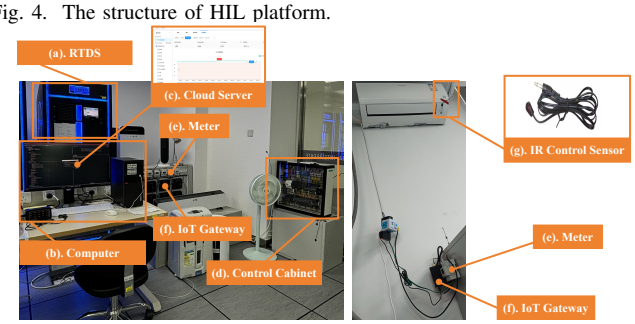

Fig. 5. Field demonstration of the HIL platform.

F. Control Optimization

Distribution system voltage regulation aims to keep the voltage operating within the security range [38]. Therefore, voltage quality is the essential factor in evaluating the effectiveness of voltage regulation. From the above analysis, the objective function of building i optimization processing can be expressed as follows:

$$\mathbf{J}_i(t) = \left\|\mathbf{X}_i(t) - \mathbf{X}_i^{\text{ref}}\right\|_{\mathbf{Q}_i}^2, \tag{24}$$

where $\mathbf{Q}_i$ is the positive definite coefficient matrix of building i. The $\mathbf{Q}_i$ implies the weight of the safety objective to be considered in the DCMPC controller optimization. $\mathbf{X}_i^{\text{ref}}$ is the reference voltage of the buildings i. Let $V_i^{\text{ref}}(t+p|t)$ represent the forecasted reference voltage of building i for step $t+p$ at moment t; And $\mathbf{X}_i^{\text{ref}}$ can be expressed as follows:

$$\mathbf{X}_i^{\text{ref}} = \left[\begin{array}{cccc} V_i^{\text{ref}}(t+1|t) & V_i^{\text{ref}}(t+2|t) & \ldots & V_i^{\text{ref}}(t+p|t) \end{array}\right]^{\mathrm{T}}. \tag{25}$$

The objective function of building i in the distribution system can be expressed as follows:

$$\min \mathbf{J}_i^{\text{o}}(t) = \min \sum_{i=1}^{M} \mathbf{J}_i(t). \tag{26}$$

The above objective function needs to satisfy the voltage and IACs constraints shown in Eqs. (17) and (18). Sequential least squares quadratic programming is a mathematical optimization technique typically used to find optimal solutions for MPC controller [39]. It can handle non-linear constraints and is suitable for the optimization problem in this study. Through the optimization algorithm, we can obtain the optimal control sequence $\mathbf{U}_i^{\text{o}}$ of building i. The first control input $\mathbf{u}_i^{\text{o}(1)}$ in the optimal control sequence $\mathbf{U}_i^{\text{o}}$ is chosen as the control result for building i. This process ensures that the control input chosen for each building is optimal within the context of the entire system's dynamics and future predictions. This method is referred to as the rolling optimization mechanism. The IoT gateway of the building i launches the consensus processing after obtaining the optimal control result to control the IACs. The building collects power changes and voltage variations through sensors and conducts the next round of rolling optimization.

G. The Convergence Analysis of the DCMPC

The Lyapunov stability theory can prove the convergence of the DCMPC. Regarding the objective function Eq. (26) of the DCMPC optimization problem as a Lyapunov function. Therefore, we can obtain the relationship as follows:

$$\begin{cases} \mathbf{J}_i^{\text{o}}(t) = 0, (\mathbf{X}_i(t) - \mathbf{X}_i^{\text{ref}}) = 0, \\ \mathbf{J}_i^{\text{o}}(t) > 0, otherwise. \end{cases} \tag{27}$$

where $(\mathbf{X}_i(t) - \mathbf{X}_i^{\text{ref}})$ is an equilibrium state of the building i. Assume that at the moment t, the optimal control sequence $\mathbf{U}_i^{\text{o}*}$ of building i corresponds to state $\mathbf{X}_i^*(t)$, and the Lyapunov function is $\mathbf{J}_i^{\text{o}*}(t)$. Assuming that the system is not suffering from any disturbance after the moment $t+p$ and the system state is equal to V_i^{sta}. The state sequence corresponding to building i at the next moment is as follows:

$$\mathbf{X}_i^*(t+1) = \left[\begin{array}{ccccc} x_i(t+2|t) & \ldots & x_i(t+p|t) & V_i^{\text{sta}} \end{array}\right]^{\mathrm{T}}. \tag{28}$$

The Lyapunov function value is updated from $\mathbf{J}_i^{\text{o}*}(t)$ to $\mathbf{J}_i^{\text{o}*}(t+1)$, which can be expressed as follows:

$$\begin{aligned} \mathbf{J}_i^{\text{o}*}(t+1) \quad &= \mathbf{J}_i^{\text{o}*}(t) - \sum_{i=1}^{M} q_i (x_i(t+1|t) - V_i^{\text{ref}}(t+1|t))^2 \\ &+ \sum_{i=1}^{M} q_i (V_i^{\text{sta}} - V_i^{\text{ref}}(t+p+1|t))^2, \end{aligned} \tag{29}$$

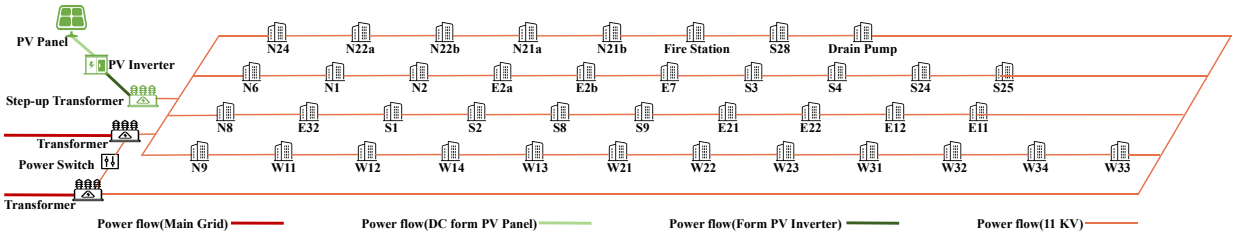

Fig. 6. A campus distribution system with 40 buildings.

where the parameter q_i belongs to $\mathbf{Q}_i$ is a positive number. The previous assumption is that there is no disturbance after the $t+p$ moment, and the error between the system state V_i^{sta} and the predicted value $V_i^{\text{ref}}(t+p+1|t)$ is close to zero. The Eq. (29) can be represented as follows:

$$\mathbf{J}_i^{\text{o}*}(t+1) \leq \mathbf{J}_i^{\text{o}*}(t). \tag{30}$$

Therefore, the rolling optimization process of DCMPC is a gradual stable process. The convergence of DCMPC is proved.

IV. Hardware-in-the-loop Experimental Platform

A. The Structure of HIL Experimental Platform

To enhance the validation of the proposed DCMPC algorithm, we have developed a HIL experimental platform. Fig. 4 shows the framework of the HIL platform, which consists of the distribution system simulation, regulation controller, and IACs management system. As shown in the structure, Fig. 4(a) is an RTDS that simulates the operation of a realistic distribution system in real time and with high accuracy. Fig. 4(b) is a computer that enables bi-directional communication with RTDS and IACs management system. The cloud server(Fig. 4(c)) can store the operating data. The main hardware in the HIL experimental platform is the IACs management system, including the control cabinet(Fig. 4(d)), meter(Fig. 4(e)), IoT gateway(Fig. 4(f)), and IR control sensor(Fig. 4(g)). Based on this HIL platform, we can realize an enhanced simulation of RTDS distribution systems with realistic IACs.

B. Distribution System Simulation

The distribution system simulation unit consists of the RTDS. RTDS performs excellently in realistically simulating the operating dynamics of the power system [40]. RTDS feeds back the operating data (node voltage and node active/reactive power) of the distribution system to the regulation controller through the HIL interface. The regulation controller can feed back the state changes of the IACs to the RTDS to update the distribution system operation state.

C. Regulation Controller

The regulation controller consists of the computer and the cloud server. The computer is regarded as a DSO that can analyse the distribution system information from RTDS and execute the proposed DCMPC algorithm to send regulation commands to the IACs management system. The proposed DCMPC algorithm will be implemented by a program written in MATLAB running on the computer. The cloud server can store the IAC's operating information, and the computer can get the IAC's operating data from the cloud service.

TABLE I
The Design of the Scenarios

	Scenario 1	***Scenario 2***
Description	PV generator unit failure.	The clouds pass through the PV panels.
Time	$50S$	$1000S$

TABLE II
Control Methods in Different Cases

Case 0	*Without regulation*
Case 1	*Utilizing the DCMPC method.*
Case 2	*Utilizing the DCMPC method, while without considering the reactive power regulation.*
Case 3	*Utilizing the DCMPC method, while without considering the heterogeneous temperature requirements of the customer.*

D. IACs Management System

The IACs management system is developed for real-time control of the IACs in the HIL experiment. This system uses IoT technology to gather real-time operating power from actual IACs. Fig. 5 is the field demonstration of the IACs management system. The DSO (i.e., computer in the regulation controller) can send commands to the control cabinet to control the IAC through the IR control sensor. The meter can collect the operating data (i.e., active power, reactive power) of the IAC and upload it to the IoT gateway. The IoT gateway uploads the operating data to the cloud service through the internet network. Based on these components, the IACs management system can aggregate IACs and respond to regulation signals from the DSO.

V. Experiment

A. Experiment Setup

The experiments are conducted based on the HIL experimental platform described in section IV. The topology diagram for the campus distribution system with 40 buildings has been designed in RTDS as shown in Fig. 6. In the experiments, the allowable voltage fluctuation range is set to $[0.95, 1.05]$ $p.u.$. The parameters of the consensus algorithm are set as $\delta_{ij} = 0.45$ and $\beta_i = 0.00095$. The DSO is set to obtain the operation status of the distribution system every 0.1 s. The control period of the DCMPC controller is set to $1s$. To better verify the proposed DCMPC algorithm's performance and voltage regulation efficiency, two scenarios are designed as shown in Table I.

a) Scenario 1: A fast voltage disturbance event occurs in the distribution system. RTDS simulates the power deficit due to PV generator failure. The deficit of active and reactive power resulted in voltage problems in the distribution system. Due to the operating reserve and inherent inertia of the

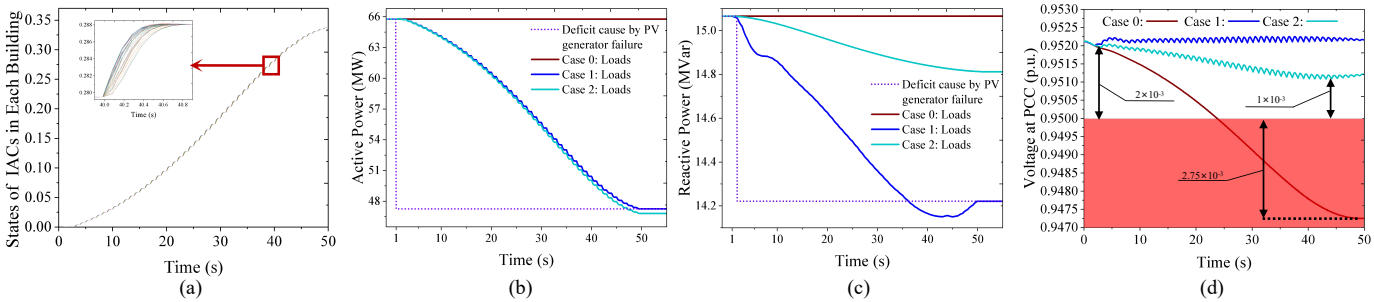

Fig. 7. The experiment results of scenario 1: (a) states of IACs in each building of Case 1; (b) total active power of the generation side and load side; (c) total reactive power of the generation side and load side; (d) voltage deviations at PCC.

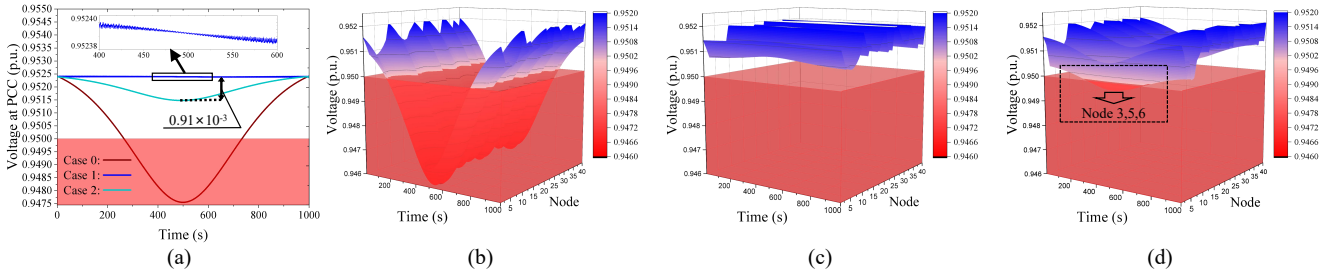

Fig. 8. The experiment results of scenario 2: (a) voltage deviations at PCC; (b) voltage deviations at each node of Case 0; (c) voltage deviations at each node of Case 1; (d) voltage deviations at each node of Case 2.

distribution system, the bus voltage does not collapse instantaneously but decreases gradually. The distribution system voltage gradually declines to the insecure range.

b) Scenario 2: A slow voltage disturbance event occurs in the distribution system. The RTDS simulates the clouds passing through the PV panels in 1000 s, which causes the voltage to drop and then recover in the distribution system.

To verify the proposed DCMPC algorithm properly, we compare four control methods in Table II. Case 0 does not perform voltage regulation for the distribution system. Case 1, Case 2, and Case 3 use the proposed DCMPC algorithm to realize voltage regulation. The difference between Case 1 and Case 2 is that Case 1 considers the reactive power regulation during the voltage regulation process while Case 2 does not. The difference between Case 1 and Case 3 is that Case 1 considers the heterogeneous temperature requirements of the customer during the voltage regulation process while Case 3 does not. In the next three subsections, the performance of the DCMPC algorithm under two scenarios and four control methods will be analyzed respectively.

B. Result Analysis of Voltage Regulation

Fig. 7(a) shows the convergence of the states of each building's IACs of Case 1 in scenario 1. It can be seen that the IAC state in each building changes and eventually stabilizes in each control period. Fig. 7(b) and (c) show the variation of active and reactive power of the generation side and load side, respectively. It can be seen that the distribution system suffers a deficit of active and reactive power at $1s$. The active and reactive power of loads in Case 0 does not change. In Case 1, the active and reactive power of the load will gradually regulate and finally close to the active and reactive power deficit of the system as shown in Fig. 7(b) and (c). Fig. 7(d) shows the variation curves of voltage at the Point of Common Coupling (PCC) under scenario 1. It can be seen from Case 0 in Fig. 7(d) that the voltage of the distribution system exceeds the security range by $2.75 \times 10^{-3} p.u.$. In contrast, Case 1 applies the proposed DCMPC algorithm to ensure the voltage operates within the security range.

Fig. 8(a) shows the variation curves of voltage at the PCC under scenario 2, i.e., the cloud passes through the PV generator. It can be observed from Case 0 in Fig. 8(a) that the voltage will drop and then rise with the shading process if there is no regulation. From Case 1 in Fig. 8(a), it can be seen that the proposed DCMPC algorithm is efficient in keeping the voltage within the normal fluctuation range.

The experimental results show that the DCMPC algorithm can dispatch IACs to maintain voltage stability when a fast or slow voltage disturbance event occurs in the distribution system.

C. Result Analysis Considering Reactive Power Regulation

Case 1 and Case 2 verify that the proposed DCMPC algorithm considering the IACs' reactive power regulation will be better than the traditional method without considering the IACs' reactive power regulation. The IACs' reactive power regulation is considered in the DCMPC algorithm of Case 1. In Case 2, the variation of IACs' reactive power follows the variation of IACs' active power as the relationship described in Eq. (3).

From the results of scenario 1 in Fig. 7(b), it can be found that Case 2 does not consider the reactive power of the IACs. It will cause the active power to exceed the system deficit to meet voltage security requirements. Although the reactive power of the IACs is regulated with the active power, the reactive power of the loads will not meet the system deficit as shown in Fig. 7(c). From the results of Fig. 7(d), it can be found that this control strategy can meet the voltage security operation

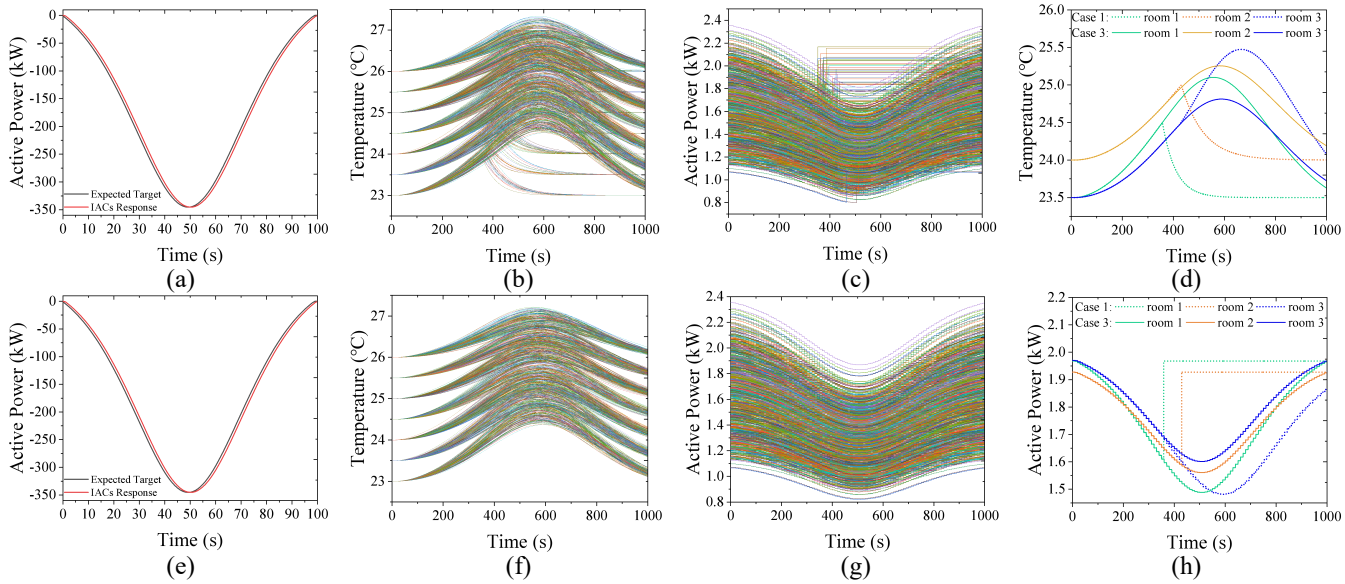

Fig. 9. The experiment results of scenario 2: (a) the response of the IACs in the building S3 to the DCMPC controller commands under the Case 1; (b) the indoor temperature of the IACs under the Case 1; (c) the active power of the IACs under the Case 1; (d) the indoor temperature of the three rooms in the building S3; (e) the response of the IACs in the building S3 to the DCMPC controller commands under the Case 3; (f) the indoor temperature of the IACs under Case 3; (g) the active power of three IACs under Case 3; (h) the active power of the three IACs in the building S3.

requirements but still has a fluctuation of $1.0 \times 10^{-3} p.u.$ compared to the normal operation state.

As for scenario 2 in Fig. 8(a), it can be seen that the proposed DCMPC algorithm used in Case 1 and Case 2 is efficient in keeping the voltage within the normal fluctuation range. However, the reactive power is not considered in Case 2 and there is a $0.91 \times 10^{-3} p.u.$ voltage fluctuation in Case 2.

To better analyze the proposed method's effectiveness, each node's voltage variation in Case $0-2$ is illustrated as shown in Fig. $8(b)-(d)$. It can be seen that both the Case 1 and Case 2 methods can improve the distribution system voltage quality. However, the voltage deviations of nodes $\{3,5,6\}$ in Case 2 still exceed the limit and suffer from under-voltage problems, as shown in the above Fig. 8(d). The experimental results show that the proposed DCMPC algorithm considering the IACs' reactive power regulation will be better than the traditional method without considering the IACs' reactive power regulation.

D. Result Analysis of Thermal Comfort for Customers

To verify the proposed DCMPC algorithm considering the thermal comfort for customers, we compare Case 1, and Case 3 under scenario 2. Case 1 and Case 3 use the proposed DCMPC algorithm to realize voltage regulation. Based on the statistical analysis of the collected data, the room outdoor temperature is assigned within the range of $30°C$ to $32°C$, while the initial indoor temperature is assigned within the range of $23°C$ to $26°C$. The maximum and minimum indoor temperature deviation is assigned within the range of $1°C$ to $3°C$. This range aligns with Fanger's PMV theory [41] where thermal comfort is achieved when temperature deviations are dynamically balanced with customer temperature requirements. Case 1 considers the customer's heterogeneous temperature requirements during the voltage regulation. When the indoor temperature exceeds the customer's setting, the IAC in Case 1 will revert to its initial operating state to maintain the indoor temperature, while Case 3 will not. A building from the distribution system is selected to explore the variations in IACs' power and temperature during the regulation process.

Fig. 9(a) and (e) illustrate the response of the IACs in building S3 of the distribution system to the DCMPC controller commands under the methods of Case 1 and Case 3, respectively. It can be observed that the actual power variation of the IACs can follow the expected trajectory. Fig. 9(b) and (f) illustrate the changes of each room's indoor temperature in building S3, respectively. It can be observed that the experiment will cause the indoor temperature to increase more than 1 °C and then decrease. While some abruptly changing curves can be observed during the regulation process in Fig. 9(b). Fig. 9(c) and (g) illustrate the variations in the active power of each IAC in building S3, respectively. From Fig. 9(c) and Fig. 9(g), it can be apparently observed that the IACs' active power follows the control command decrease and then increase. While some abruptly changing curves can be observed during the regulation process in Fig. 9(c).

Fig. 9(d) and (h) illustrate the variations of three rooms' indoor temperatures and the active power of the IACs in building S3, respectively. The customers in room 1 and room 2 set the allowable indoor temperature deviation is 1 °C, while room 3 is 3 °C. As shown in Fig. 9(d), the IAC of room 1 and room 2 in Case 1 will not follow the control command when the indoor temperature exceeds 1 °C. Since the customer's heterogeneous temperature requirements, the IACs of room 1 and room 2 in Case 1 will revert to their initial active power to ensure the indoor temperature remains at its initial level, as shown in Fig. 9(h). The indoor temperature of these rooms gradually reverts to its initial temperature in Case 1 due to the customer's heterogeneous temperature requirements. The DCMPC's consensus process and rolling optimization mechanism can compensate the power deficit of

room 1 and 2 in real-time and allows room 3 to provide more power to ensure that building S3 meets the system's power requirements, as shown in Fig. 9(h).

From the above analysis, it can be observed that the proposed DCMPC algorithm considers the customer's heterogeneous temperature requirements. The consensus processing enables the IACs to adjust their power demand based on indoor temperature during the voltage regulation process. It can ensure the indoor temperature is within the customer comfort requirement, thereby achieving thermal comfort. The distribution system voltage can reach a consensus security state finally.

VI. Conclusion

Distribution system voltage violation problems are severely challenged by the gradually increasing penetration of distributed renewable energies. IACs can provide voltage regulation services to the distribution system if they can be aggregated and regulated. This paper proposes DCMPC algorithms to coordinate the active and reactive power of IACs to participate in voltage regulation and achieve good thermal comfort for customers. The HIL experiments show that the proposed DCMPC algorithm can maintain the voltage within the security range. The proposed DCMPC algorithm considering both IACs' active and reactive power offers 50% security margin more than the traditional regulation without considering the reactive power. Consesus-based processing of IACs with distributed features allows the IACs to be appropriately scheduled to respond to the regulation signals. The thermal comfort for customers, i.e., the heterogeneous indoor temperature requirements of the customer, is also considered in the regulation process. The proposed DCMPC algorithm greatly improves the efficiency of the voltage regulation of the distribution system.

References

[1] K. Utkarsh, F. Ding, X. Jin, M. Blonsky, H. Padullaparti, and S. P. Balamurugan, "A network-aware distributed energy resource aggregation framework for flexible, cost-optimal, and resilient operation," *IEEE Transactions on Smart Grid*, vol. 13, no. 2, pp. 1213–1224, 2021.

[2] Y. Lu, M. Fu, J. Gao, Q. Shi, and W. Liu, "Voltage limit violation risk evaluation method considering communication failures in distributed voltage regulation system," *International Journal of Electrical Power & Energy Systems*, vol. 147, p. 108886, 2023.

[3] W. Zhang, C. Zhang, J. Li, L. Zhu, S. Cao, W. Huang, and Z. Shuai, "Multi-resource collaborative service restoration of a distribution network with decentralized hierarchical droop control," *Protection and Control of Modern Power Systems*, vol. 9, no. 1, pp. 19–37, 2024.

[4] A. S. Yadav and V. Mukherjee, "Conventional and advanced pv array configurations to extract maximum power under partial shading conditions: A review," *Renewable Energy*, vol. 178, pp. 977–1005, 2021.

[5] M. Alrashidi and S. Rahman, "A bi-level optimization method for voltage control in distribution networks using batteries and smart inverters with high wind and photovoltaic penetrations," *International Journal of Electrical Power & Energy Systems*, vol. 151, p. 109217, 2023.

[6] N. Mahmud and A. Zahedi, "Review of control strategies for voltage regulation of the smart distribution network with high penetration of renewable distributed generation," *Renewable and Sustainable Energy Reviews*, vol. 64, pp. 582–595, 2016.

[7] X. Zhang, M. Pipattanasomporn, T. Chen, and S. Rahman, "An iot-based thermal model learning framework for smart buildings," *IEEE Internet of Things Journal*, vol. 7, no. 1, pp. 518–527, 2019.

[8] Z. Ji, X. Liu, and D. Tang, "Game-theoretic applications for decision-making behavior on the energy demand side: a systematic review," *Protection and Control of Modern Power Systems*, vol. 9, no. 2, pp. 1–20, 2024.

[9] X. Zhang, D. Biagioni, M. Cai, P. Graf, and S. Rahman, "An edge-cloud integrated solution for buildings demand response using reinforcement learning," *IEEE Transactions on Smart Grid*, vol. 12, no. 1, pp. 420–431, 2020.

[10] M. Wang, Y. Mu, F. Li, H. Jia, X. Li, Q. Shi, and T. Jiang, "State space model of aggregated electric vehicles for frequency regulation," *IEEE Transactions on Smart Grid*, vol. 11, no. 2, pp. 981–994, 2019.

[11] Q. Xie, H. Hui, Y. Ding, C. Ye, Z. Lin, P. Wang, Y. Song, L. Ji, and R. Chen, "Use of demand response for voltage regulation in power distribution systems with flexible resources," *IET Generation, Transmission & Distribution*, vol. 14, no. 5, pp. 883–892, 2020.

[12] C. Gao, M. Song, S. Ma, M. Guo, R. Lv, and F. Fei, "Dynamic modelling and optimal control of virtual power plant driven by commercial hvacs," *IET Renewable Power Generation*, vol. 16, no. 12, pp. 2590–2603, 2022.

[13] H. Hui, Y. Ding, T. Chen, S. Rahman, and Y. Song, "Dynamic and stability analysis of the power system with the control loop of inverter air conditioners," *IEEE Transactions on Industrial Electronics*, vol. 68, no. 3, pp. 2725–2736, 2021.

[14] Y. Hua, Q. Xie, H. Hui, Y. Ding, W. Wang, H. Qin, X. Shentu, and J. Cui, "Collaborative voltage regulation by increasing/decreasing the operating power of aggregated air conditioners considering participation priority," *Electric Power Systems Research*, vol. 199, p. 107420, 2021.

[15] Y. Hua, Q. Xie, H. Hui, Y. Ding, J. Cui, and L. Shao, "Use of inverter-based air conditioners to provide voltage regulation services in unbalanced distribution networks," *IEEE Transactions on Power Delivery*, vol. 38, no. 3, pp. 1569–1579, 2023.

[16] Y. Wang, Y. Xu, Y. Tang, K. Liao, M. H. Syed, E. Guillo-Sansano, and G. M. Burt, "Aggregated energy storage for power system frequency control: A finite-time consensus approach," *IEEE Transactions on Smart Grid*, vol. 10, no. 4, pp. 3675–3686, 2018.

[17] Z. Zheng, R. Tang, X. Luo, H. Li, and S. Wang, "A distributed coordination strategy for heterogeneous building flexible thermal loads in responding to smart grids," *IEEE Transactions on Smart Grid*, 2023.

[18] Y. Wang, Y. Tang, Y. Xu, and Y. Xu, "A distributed control scheme of thermostatically controlled loads for the building-microgrid community," *IEEE Transactions on Sustainable Energy*, vol. 11, no. 1, pp. 350–360, 2020.

[19] J. Hong, H. Hui, H. Zhang, N. Dai, and Y. Song, "Distributed control of large-scale inverter air conditioners for providing operating reserve based on consensus with nonlinear protocol," *IEEE Internet of Things Journal*, vol. 9, no. 17, pp. 15 847–15 857, 2022.

[20] N. Zhao, D. Yue, C. Dou, and T. Shi, "Distributed dynamic event-triggered cooperative control of multiple tcls and hess for improving frequency regulation," *IEEE Transactions on Industrial Informatics*, 2023.

[21] Z. Zheng, S. Wang, W. Li, and X. Luo, "A consensus-based distributed temperature priority control of air conditioner clusters for voltage regulation in distribution networks," *IEEE Transactions on Smart Grid*, vol. 14, no. 1, pp. 290–301, 2022.

[22] X. Zhu, J. Wang, N. Lu, N. Samaan, R. Huang, and X. Ke, "A hierarchical vlsm-based demand response strategy for coordinative voltage control between transmission and distribution systems," *IEEE Transactions on Smart Grid*, vol. 10, no. 5, pp. 4838–4847, 2018.

[23] J. Hu, C. Ye, Y. Ding, J. Tang, and S. Liu, "A distributed mpc to exploit reactive power v2g for real-time voltage regulation in distribution networks," *IEEE Transactions on Smart Grid*, vol. 13, no. 1, pp. 576–588, 2021.

[24] W. Viriyautsahakul, W. Panacharoenwong, W. Pongpiriyakijkul, S. Kosolsaksakul, and W. Nakawiro, "A simulation study of inverter air conditioner controlled to supply reactive power," *Procedia Computer Science*, vol. 86, pp. 305–308, 2016.

[25] N. Zhao, S. Gorbachev, D. Yue, V. Kuzin, C. Dou, X. Zhou, and J. Dai, "Model predictive based frequency control of power system incorporating air-conditioning loads with communication delay," *International Journal of Electrical Power & Energy Systems*, vol. 138, p. 107856, 2022.

[26] M. Chen, J. Zhao, Z. Xu, Y. Liu, Y. Zhu, and Z. Shao, "Cooperative distributed model predictive control based on topological hierarchy decomposition," *Control Engineering Practice*, vol. 103, p. 104578, 2020.

[27] Z. Zhang, D. Yue, and C.-X. Dou, "Dmpc-based coordinated voltage control for integrated hybrid energy system," *IEEE Transactions on Industrial Informatics*, vol. 17, no. 10, pp. 6786–6797, 2020.

[28] A. L. da Fonseca, K. M. Chvatal, and R. A. Fernandes, "Thermal comfort maintenance in demand response programs: A critical review," *Renewable and Sustainable Energy Reviews*, vol. 141, p. 110847, 2021.

[29] L. Chen and H. Hui, "Model predictive control-based active/reactive power regulation of inverter air conditioners for improving voltage quality of distribution systems," *IEEE Transactions on Industrial Informatics*, 2024.
[30] H. Hui, P. Siano, Y. Ding, P. Yu, Y. Song, H. Zhang, and N. Dai, "A transactive energy framework for inverter-based hvac loads in a real-time local electricity market considering distributed energy resources," *IEEE Transactions on Industrial Informatics*, vol. 18, no. 12, pp. 8409–8421, 2022.
[31] T. Inoue, H. Doi, and T. Miyajima, "Electrolytic capacitor-less inverter technology for miniaturization of air conditioning system," in *2022 International Power Electronics Conference (IPEC-Himeji 2022-ECCE Asia)*. IEEE, 2022, pp. 667–672.
[32] Y.-J. Kim, E. Fuentes, and L. K. Norford, "Experimental study of grid frequency regulation ancillary service of a variable speed heat pump," *IEEE Transactions on Power Systems*, vol. 31, no. 4, pp. 3090–3099, 2015.
[33] M. Song, C. Gao, H. Yan, and J. Yang, "Thermal battery modeling of inverter air conditioning for demand response," *IEEE Transactions on Smart Grid*, vol. 9, no. 6, pp. 5522–5534, 2017.
[34] T. Endo, K. Satodate, K. Ishida, M. Kanamori, K. Okada, K. Kogetsu, and H. Higashiji, "Power electronics technology applied in inverter air conditioners," in *2020 23rd International Conference on Electrical Machines and Systems (ICEMS)*. IEEE, 2020, pp. 2095–2100.
[35] D. Das, S. Mishra, and B. Singh, "An aggregated energy management methodology for air conditioning system with dab converter," *IEEE Journal of Emerging and Selected Topics in Industrial Electronics*, vol. 3, no. 1, pp. 124–132, 2021.
[36] T. Ding, C. Li, Y. Yang, R. Bo, and F. Blaabjerg, "Negative reactance impacts on the eigenvalues of the jacobian matrix in power flow and type-1 low-voltage power-flow solutions," *IEEE Transactions on Power Systems*, vol. 32, no. 5, pp. 3471–3481, 2016.
[37] J. Hong, H. Hui, H. Zhang, N. Dai, and Y. Song, "Event-triggered consensus control of large-scale inverter air conditioners for demand response," *IEEE Transactions on Power Systems*, vol. 37, no. 6, pp. 4954–4957, 2022.
[38] Y. Wang, L. Von Krannichfeldt, T. Zufferey, and J.-F. Toubeau, "Short-term nodal voltage forecasting for power distribution grids: An ensemble learning approach," *Applied Energy*, vol. 304, p. 117880, 2021.
[39] H. J. Ferreau, H. G. Bock, and M. Diehl, "An online active set strategy to overcome the limitations of explicit mpc," *International Journal of Robust and Nonlinear Control: IFAC-Affiliated Journal*, vol. 18, no. 8, pp. 816–830, 2008.
[40] B. Cui, A. K. Srivastava, and P. Banerjee, "Synchrophasor-based condition monitoring of instrument transformers using clustering approach," *IEEE Transactions on Smart Grid*, vol. 11, no. 3, pp. 2688–2698, 2019.
[41] M. Luo, K. Jiang, J. Wang, W. Feng, L. Ma, X. Shi, and X. Zhou, "Data-driven thermal preference prediction model with embodied air-conditioning sensors and historical usage behaviors," *Building and Environment*, vol. 220, p. 109269, 2022.